THE UNIVERSITY OF TRANS-DISCIPLINARY HEALTH SCIENCES AND TECHNOLOGY

Private University Established in Karnataka by ACT 35 of 2013

BENGALURU - 560064

Structural and Biochemical studies of the Cullin3 complex with the N-terminal domain of Kelch-like ECH associated protein (Keap1) associated with the Neurological diseases and PlyGRCS endolysin towards the treatment of MRSA infections

PhD Synopsis

Gopinatha Krishnappa

Guide
Dr. S. Thiyagarajan
Associate Professor
Institute of Bioinformatics and Applied Biotechnology (IBAB)

Joint Guide
Dr. B. Padmanabhan
Professor and Head
Department of Biophysics
National Institute of Mental Health and Neurosciences (NIMHANS)

THE UNIVERSITY OF TRANS-DISCIPLINARY HEALTH SCIENCES AND TECHNOLOGY

Private University Established in Karnataka by ACT 35 of 2013

BENGALURU - 560064

PhD SYNOPSIS

Name of the candidate	**Gopinatha Krishnappa**
Date of Joining	18th February 2019
Date of Registration	18th February 2019
Registration No.	PHD/R/2019-20/1501(**20219021501**)
Thesis Title	**Structural and Biochemical studies of the Cullin3 complex with the N-terminal domain of Kelch-like ECH associated protein (Keap1) associated with the Neurological diseases and PlyGRCS endolysin towards the treatment of MRSA infections**
Name of the Guide	**Dr. S. Thiyagarajan** Associate Professor, IBAB, Electronic City Phase I, Bengaluru – 560100
Name of the Co-Guide	**Dr. B. Padmanabhan** Professor and Head Department of Biophysics, NIMHANS, Bengaluru – 560029
Internal Member	**Dr. Kshitish K Acharya** Professor, IBAB, Electronic City Phase I, Bengaluru 560 100
External Member	**Dr. Gurunathan Jayaraman** Professor, School of Bio Science & Technology Vellore Institute of Technology, Vellore 632 014

Signature of the candidate

Signature of the guide

Signature of the co-guide

Signature of internal member

Signature of the external member

PART A – THE KEAP1-CULLIN3 SYSTEM

CHAPTER-1: INTRODUCTION

Maintaining cellular homeostasis is a vital process for cells to function normally and efficiently. The cell's homeostatic conditions are altered by both exogenous as well as endogenous factors that produce reactive oxygen species (ROS) and other hyper-reactive electrophiles. The overburden of ROS results in oxidative stress (Kohen & Nyska., 2002) and various pathophysiological conditions such as cancer, metabolic diseases, and various neurodegenerative diseases (Noh & Ha., 2011).

The Keap1-Nrf2 system plays a central role in protecting cells against oxidative and xenobiotic stress (Ishii *et al*., 2000; Deshmukh et al., 2017). The Nrf2 is a transcription factor that activates several cytoprotective genes via an antioxidant response element (Marzec et al.., 2007). Under homeostatic/unstressed conditions, the cellular concentration of Nrf2 remains low, and it is modulated by Keap1 (Kelch-like ECH-associated protein 1) that assists Nrf2 degradation through the proteasomal pathway (Itoh *et al*., 2004). Due to oxidative stress, Nrf2 dissociates from Keap1. As a result, Nrf2 will translocate to the nucleus, where it dimerizes with a small Maf protein and acts upon the ARE in the regulatory region of its target genes essential for ROS-neutralizing enzymes and proteins (Cleasby *et al*., 2014). The Keap1 protein is a well-established new therapeutic drug target for Parkinson's disease (PD).

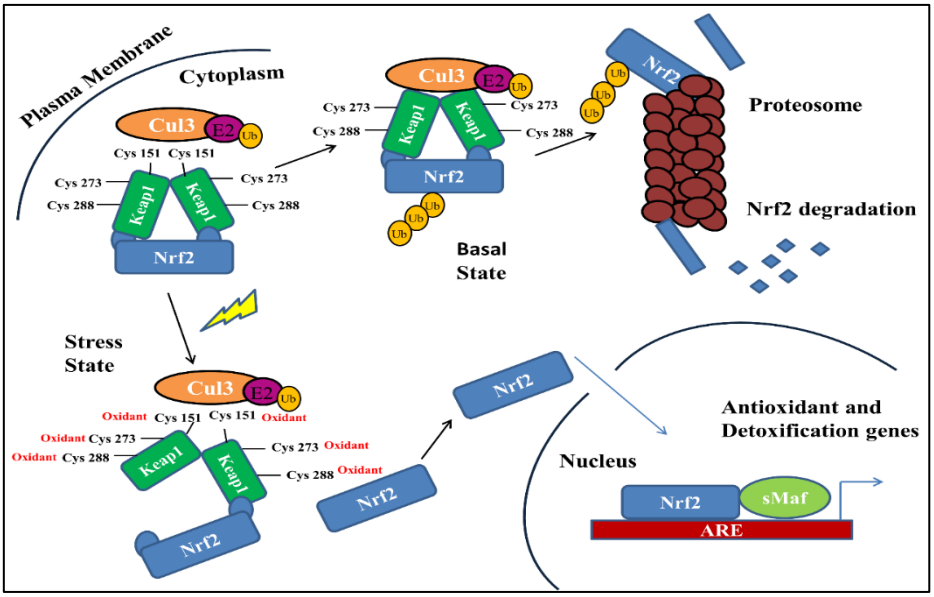

Figure 1.1: Keap1-Nrf2 pathway in basal and stress state conditions.

Parkinson's disease (PD) is characterized by the loss of dopaminergic neurons in a brain region known as the substantia nigra (SN) and the presence of α-synuclein-containing inclusion bodies (Lewy bodies) in the cytoplasm of neurons (Mosley *et al*., 2006). Activation of the Nrf2-ARE system in PD has been demonstrated by up-regulation of regulated proteins including NQO1 (NAD(P)H quinone oxidoreductase) and HO-1(heme oxygenase-1) (Riedl *et al*., 1999) which will neutralize the ROS levels.

The thesis work of the author provides insights into:

1. Identification of pivotal residues involved in the interaction of BTB-IVR - Cullin3 protein complex.
2. Structure-function analysis of BTB domain and BTB-ligand complex and screening of small inhibitor molecules of BTB domain of Keap1 by rational approach.
3. The development of small inhibitors against the BTB domain which in turn increases the Nrf2 activation in Parkinson's disease model.

The current results provide a valuable understanding of the molecular mechanism of the Keap1-Nrf2-Cullin3 complex in the homeostatic condition and also in the identification of small molecule inhibitors against the BTB domain of Keap1 for the Nrf2 activation.

OBJECTIVES OF THE STUDY:

1. ***Identification of critical residues involved in the interaction of Keap1 BTB-IVR – Cullin3 protein complex***

a) Cloning, expression, and purification of Keap1 BTB-IVR - Cullin3 from *E. coli* system.
b) Identification of critical residues involved in the interaction of Keap1 BTB-IVR – Cullin3 protein complex by site-directed mutagenesis.
c) Binding studies of Keap1 BTB domain and Cullin3 by using Surface Plasmon resonance and Micro-scale Thermophoresis.
d) In-vitro binding assay to check the interaction of Keap1 BTB domain and Cullin3 protein
e) Cell line studies on wild and mutant Cullin3 by Ubiquitination assay

2. ***Structure and function analysis of the BTB domain of Keap1 and Identification of novel inhibitors by rational approach***

a) Cloning, expression, and purification of BTB domain of Keap1 protein from *E. coli* system
b) Biochemical screening of small molecule inhibitors and phytochemicals for the BTB domain of Keap1 by SPR and MST
c) Crystallization, X-ray diffraction, data collection, 3D structures determination and analysis of BTB domain and BTB domain-inhibitor complex(s).
d) Identification of critical residues involved in the interaction of BTB domain-inhibitor complex by site-directed mutagenesis.

3. ***Determination of the effect of selected small molecule inhibitors on Nrf2 activation by using neuronal cell lines (SHSY5Y) in the Parkinson's disease (PD) model.***

CHAPTER - 2: MATERIAL AND METHODS

E. coli DH5α cells were grown in LB media with respective antibiotics for cloning and site-directed mutagenesis of recombinant genes (BTB, BTBIVR domain, and Cullin3). Clone confirmation was done by sequencing. Expression hosts, BL21 codon plus, and Rosetta *E. coli* cells were used for protein expression, followed by the production of BTB, BTBIVR, and Cullin3 proteins (wild type & mutants) were performed by series of chromatographic techniques to get pure proteins. Protein homogeneity and stability were checked by Dynamic light scattering and Tycho.

The purified BTBIVR and Cullin3 (wild type and mutants) proteins were used for interaction studies by Microscale thermophoresis (MST) and in vitro assays. The elutes from in vitro assays were taken for western blots to check for the proteins' specificity.

Phytochemicals were extracted from medicinal plants using the Soxhlet method. Initial binding studies for the extracts with the BTB domain were performed by Surface plasmon resonance (SPR). Docking and molecular simulations were carried out for the synthetic compounds and phytochemicals from the extract with the BTB domain of Keap1 protein. Binding studies were performed for the BTB, Cullin3, synthetic compounds, and phytochemical extract by MST, SPR, and invitro assays. Competitive inhibition was done for the BTB-Cullin3 complex formation by using synthetic compounds and phytochemical extract. Protein crystallization was carried out for the BTB domain and synthetic compounds by using hanging drop crystallization. X-ray diffraction, data collection, and structure determination of BTB domain-ligand complex was done.

Cell line studies were carried out for the small molecule inhibitors and phytochemical extract by using N27 dopaminergic neuronal cells for the Nrf2 activation. The effect of the inhibitor molecule and phytochemical extract was assessed by cell viability or MTT assay in N27 neuroblastoma cells using 3-(4,5-dimethylthiazol-2-yl)-2,5-diphenyltetrazolium bromide. A few cycles of passaging of N27 cells were carried out in T75 flasks. After reaching 80% confluency, cells were treated with an Oxidant (Rotenone), an inhibitor molecule, and a phytochemical extract. Later, treated cells were harvested to check the expression of antioxidant enzymes. To evaluate the effect of the selected inhibitor molecule and phytochemical extract at the transcriptional level (qRT-PCR) and translation level (Western blot) of Nrf2 downstream enzymes like Glutamate-cysteine ligase (GCLC), NAD(P)H oxidoreductase (NQO1), and heme-oxygenase (HO-1) were analyzed.

CHAPTER - 3: RESULTS AND DISCUSSION

OBJECTIVE 1:

All the proteins were expressed on a large scale for protein purification. The size of the BTBIVR domain and Cullin3 proteins are 17 kDa and 45 kDa respectively which has been seen on SDS-PAGE. The purified protein was concentrated and used for the biochemical, and *in-vitro* studies.

MST was performed for the BTBIVR and Cullin3 (wild type & mutant) proteins and affinity was determined. Due to mutation in the cullin3 protein, Q56, R59 cullin3 mutants showed a 2-fold change in affinity, Y58 cullin3 mutant showed a 3-fold change in affinity, Y62, K68 cullin3 mutants showed a 4-5-fold change in affinity and Y125 cullin3 mutant showed no or weak binding as compared with the wild type cullin3 complex with BTBIVR protein **(Figure 3.1)**. A pull-down assay was carried out to check the interaction between BTB, BTBIVR, and cullin3 proteins. A 1:1 ratio of Cullin3: BTBIVR proteins were taken and the assay was carried out. Elutes showed both the proteins on the gel; which confirmed the interaction between the proteins.

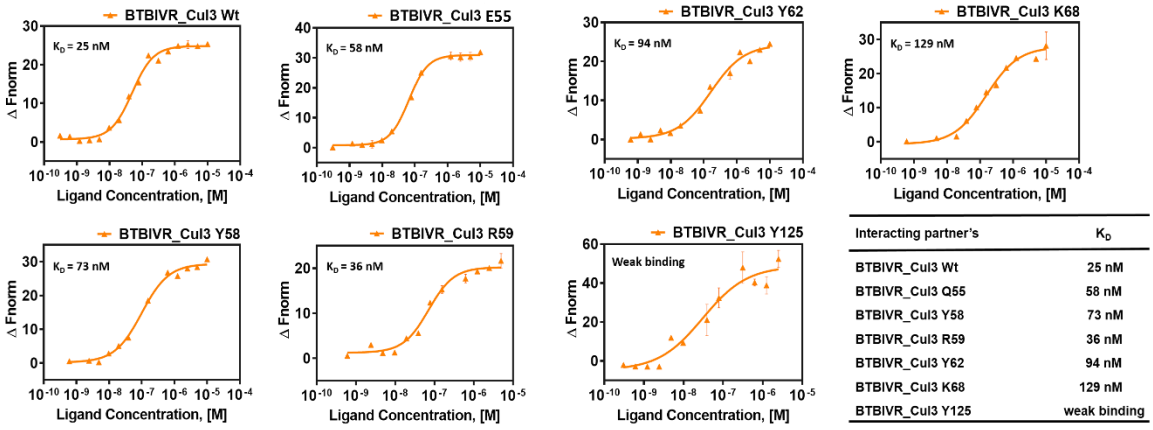

Interacting partner's	K_D
BTBIVR_Cul3 Wt	25 nM
BTBIVR_Cul3 Q55	58 nM
BTBIVR_Cul3 Y58	73 nM
BTBIVR_Cul3 R59	36 nM
BTBIVR_Cul3 Y62	94 nM
BTBIVR_Cul3 K68	129 nM
BTBIVR_Cul3 Y125	weak binding

Figure 3.1: The quantitative binding analysis of BTBIVR and Cullin3 proteins. Binding curves for the interactions of fluorescently labeled *BTBIVR* with wild-type and mutant Cullin3 proteins were shown as the change in normalized fluorescence (ΔFnorm). The K_D values are summarized in the Table. The K_D values were obtained after fitting the binding curves between ΔF_{norm} plotted as a function of the ligand concentration.

OBJECTIVE 2:

All the proteins were expressed on a large scale for protein purification. The size of the BTB and Cullin3 proteins are 14 kDa and 45 kDa respectively which has been verified on a SDS-PAGE. The purified protein was concentrated and used for the crystallization, biochemical, and *in-vitro* studies.

Co-crystallization of BTB (S172A) domain protein with the compound was tried, crystals were grown in 0.2 M lithium acetate, 18-20% PEG 3350, and 1mM TCEP within 10 days. Diffraction of crystals was done. X-ray diffraction, data collection, and structure determination were carried out. The same parameters were followed to solve the S172A BTB mutant protein for analysis of the structure; only apo BTB protein was visible, and there was no density for the compound in the binding region of the BTB.

The biochemical studies were performed for BTB and cullin3, the selected Phenanthridine compounds (Am-702 & Am-766), and *Nardostachys jatamansi* extracts against the BTB protein by using MST (binding and competitive binding) and SPR **(Figure 3.2)**. The binding affinity was determined for the BT and Cullin3. The MST assay was performed to determine the binding affinity of Am-702 & Am-766 with BTB protein was found to be 353 nM & 9.44 µM respectively. Competitive inhibition between BTB-compound and BTB-extract with Cullin3 yielded binding affinity of 3.47 µM and 1.2 µM respectively.

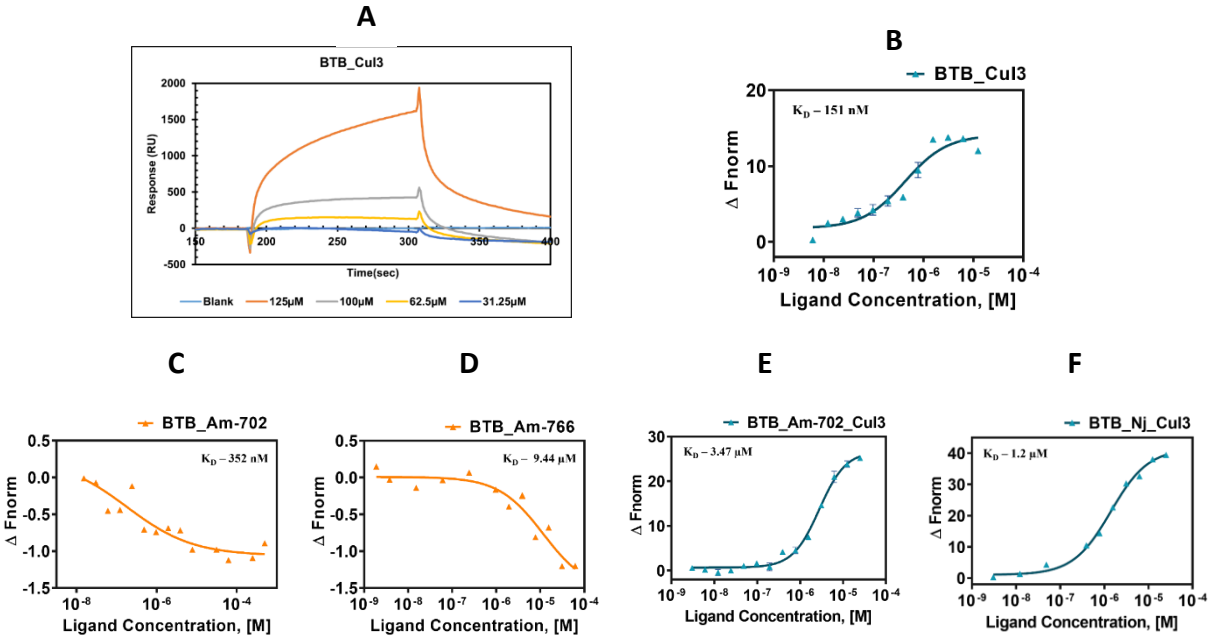

Figure 3.2: The quantitative binding analysis of BTB, Cullin3, Am compounds, and Nj extract. **A.** Sensorgram for the binding of molecules with BTB immobilized on a CM5 chip was obtained at a different concentration of Cullin3. Binding curves for the interactions of fluorescently labeled *BTB* with **B.** Cullin3, **C.** Am-702, **D.** Am-766, **E.** BTB-Am-702_Cullin3 and **F.** BTB-Nj_Cullin3 were shown as the change in normalized fluorescence (ΔFnorm). The K_D values were obtained after fitting the binding curves between ΔF_{norm} plotted as a function of the ligand concentration.

OBJECTIVE 3:

- **Effect of Am-702 compound and *Nardostachys jatamansi* extract on N27 cells**

The effect of the Am-702 compound and NJ extract was assessed by cell viability in N27 neuroblastoma cells using 3-(4,5-dimethylthiazol-2-yl)-2,5-diphenyltetrazolium bromide (MTT assay). To investigate the effect of Am-702 and Nardostachys jatamansi extract on protein expression levels of GCLC, NQO1, HO-1, and GLUR western blot was performed. From western blot analysis, it is evident that the Am-702 compound upregulated the expression levels of GCLC and NQO1 **(Figure 3.3)**, and the *Nj* extract upregulated the expression levels of HO-1 and GLUR **(Figure 3.4)**, which reveals the cell protection by antioxidant enzymes. Indicating Am-702 compound and *Nj* extract phytochemicals competitively binding to the Keap1 protein and free the Nrf2 to activate the ARE driven antioxidant enzymes.

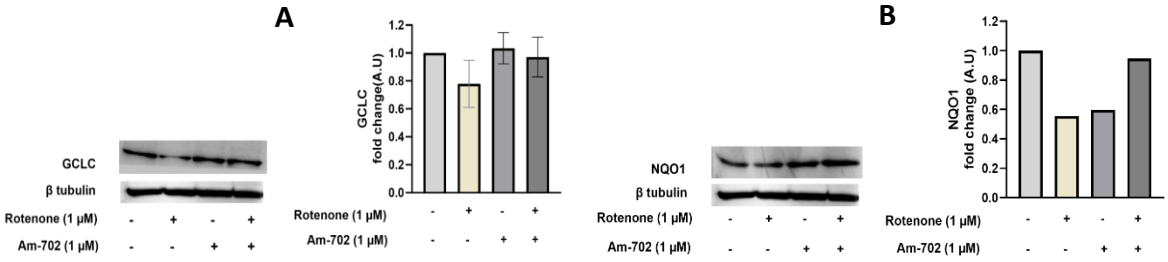

Figure 3.3: Effect of Am-702 on the protein expression level of GCLC and NQO1. Immunoblot analysis represents an increase in the **A.** GCLC and **B.** NQO1 protein expression level after treatment with Am-702 compound (1µM).

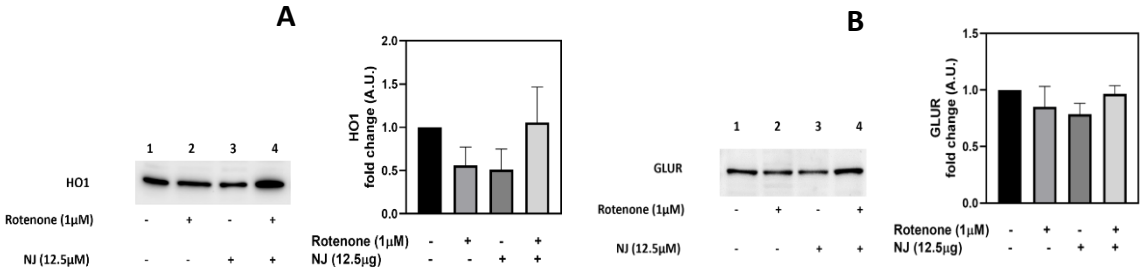

Figure 3.4: Effect of Nj extract on the protein expression level of HO-1 and GLUR. Immunoblot analysis represents an increase in the **A.** HO-1 and **B.** GLUR protein expression level after treatment with Nj extract (12.5 µg).

CHAPTER -4: CONCLUSION

The interaction studies between BTBIVR and cullin3 (wild-type and mutants) proteins showed binding affinities for BTBIVR-Cullin3 wild-type, E55, Y58, R59, Y62, K68 & Y125 mutants of 25 nM, 58 nM, 73 nM, 36 nM, 94 nM, 129 nM, and weak binding respectively. These established the importance of novel residues involved in the interaction of the BTBIVR and Cullin3 protein complex. Further, an in vitro assay between BTBIVR and Cullin3 showed the interaction between them.

The interaction studies of BTB and Cullin3 proteins showed binding affinities of 151 nM and 11.3 µM by MST and SPR respectively; which indicated a strong protein complex formation between them. Further, binding studies were carried out between inhibitor molecules with the BTB domain of Keap1. The binding affinity of Am-702 & Am-766 with BTB protein was found to be 353 nM & 9.44 µM respectively; Am-702 showed strong affinity towards BTB protein which could be a novel inhibitor as compared with AM-766. Competitive inhibition between BTB-compound and BTB-extract with Cullin3 showed binding affinity of 3.47 µM and 1.2 µM respectively; which conferred inhibition of BTB-Cullin3 complex formation.

Based on biochemical studies, Am-702 and phytochemical extract showed better binding to the BTB domain pf Keap1. Therefore, Am-702 and the phytochemical extract were taken for the cell-based assays to check its effect on rotenone-induced neurotoxic N27 neuronal cells. The effect of inhibitors on N27 cells showed an increase in the expression of anti-oxidant enzymes which showed that inhibitors and phytochemicals can bind to the Keap1 which will disturb Cullin3 to interact with it and also enable the Nrf2 to dissociate from the Keap1. Further, Nrf2 will translocate to the nucleus to transcribe the anti-oxidant genes which will neutralize the ROS levels in the cells.

REFERENCES:

1. Kohen, Ron, and Abraham Nyska. Invited review: Oxidation of biological systems: oxidative stress phenomena, antioxidants, redox reactions, and methods for their quantification. *Toxicologic pathology*, (2002). 30.6: 620-650.
2. Noh, Hyunjin, and Hunjoo Ha. "Reactive oxygen species and oxidative stress." *Diabetes and the Kidney*, (2011). 170: 102-112.

3. Ishii, Tetsuro, et al. Transcription factor Nrf2 co-ordinately regulates a group of oxidative stress-inducible genes in macrophages. *Journal of Biological Chemistry*, (2000). 275.21: 16023-16029.
4. Deshmukh, P., Unni, S., Krishnappa, G., & Padmanabhan, B. The Keap1–Nrf2 pathway: promising therapeutic target to counteract ROS-mediated damage in cancers and neurodegenerative diseases. *Biophysical reviews*, (2017). *9*(1), 41-56.
5. Marzec JM, Christie JD, Reddy SP, Jedlicka AE, Vuong H, Lanken PN, Aplenc R, Yamamoto T, Yamamto M, Cho HY, Kleeberger SR. Functional polymorphisms in the transcription factor Nrf2 in humans increase the risk of acute lung injury. FASEB J (2007). 21(9): 2237 - 2246
6. Itoh, Ken, Kit I. Tong, and Masayuki Yamamoto. Molecular mechanism activating Nrf2–Keap1 pathway in the regulation of adaptive response to electrophiles. *Free Radical Biology and Medicine*, (2004). 36.10: 1208-1213
7. Cleasby, A., Yon, J., Day, P. J., Richardson, C., Tickle, I. J., Williams, P. A., ... & Qi, H. Structure of the BTB domain of Keap1 and its interaction with the triterpenoid antagonist CDDO. *PloS one*, (2014). 9(6):e98896.
8. Mosley, R. L., Benner, E. J., Kadiu, I., Thomas, M., Boska, M. D., Hasan, K., & Gendelman, H. E. Neuroinflammation, oxidative stress, and the pathogenesis of Parkinson's disease. *Clinical neuroscience research*, (2006). 6(5): 261-281.
9. Riedl, Andrew G., Paul M. Watts, Catherine T. Brown, and Peter Jenner. P450 and heme oxygenase enzymes in the basal ganglia and their roles in Parkinson's disease. *Advances in neurology*, (1999). 80: 271-286.

PART- B: PLYGRCS ENDOLYSIN TOWARDS THE TREATMENT OF MRSA INFECTIONS

CHAPTER - 5: INTRODUCTION

The emergence of antibiotic-resistant bacterial strains has become problematic in modern medicine. About 70% of the bacteria that cause hospital-acquired infections are resistant to one or more antibiotics. *Staphylococcus aureus* is a gram-positive pathogenic bacterium that has resistance against antibiotics and is a major cause of skin infections, food poisoning, and life-threatening diseases such as pneumonia, endocarditis, and septicemia. As a result, clinicians and researchers are interested in developing novel and effective approaches for treating infection caused by multidrug-resistant bacteria are specific in targeting and eliminating bacteria by their lytic bacteriophages. (Daniel C et al, 2015).

The peptidoglycan hydrolases cleave various covalent bonds of bacterial peptidoglycan. Peptidoglycan hydrolases are identified in bacteria, phages, and some eukaryotes (Parisien *et al*, 2008). Enzybiotics/peptidoglycan hydrolases/lysins are enzymes released by bacteriophages during the lytic cycle of viral infection. The peptidoglycan hydrolases are efficient in killing bacteria when applied exogenously. The lytic activity of PlyGRCS depends on the presence of a co-factor, calcium. (Linden *et al*. 2015). PlyPy endolysin displayed the highest activity in the presence of calcium at a neutral pH. (Lood *et al*, 2014), and LysGH15 depends on calcium ions for their lytic activity (Gu *et al*, 2014).

PhageGRCS endolysin has antibacterial activity and kills a wide range of pathogenic bacteria; directly acts on the peptidoglycan layer of the bacteria, therefore they are termed “Enzybiotics”. These are alike antibiotics; which can be used for the treatment of bacterial infections. Therefore, phage therapy is more effective than antibiotics in the treatment of pathogenic bacterial species. The *PhageGRCS* endolysin has an N-terminal CHAP catalytic domain and a C-terminal SH3b binding domain. This study enables us to elucidate the 3D structural details of the PhageGRCS protein and also important residues present in the CHAP domain which are involved in the lytic activity against Methicillin-resistant *Staphylococcus aureus* (MRSA) strains.

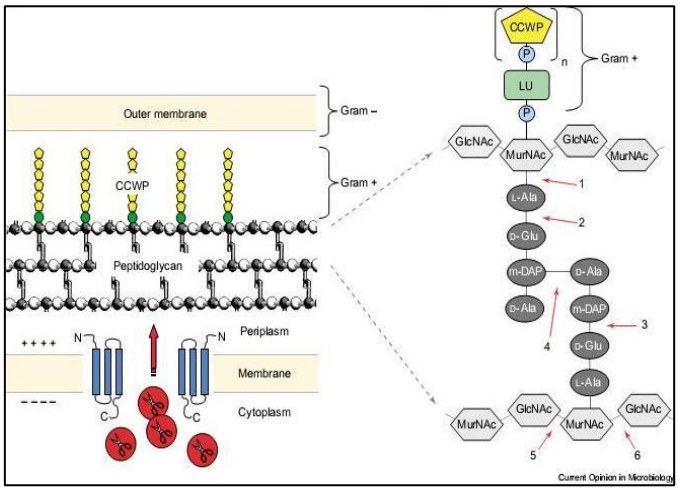

Figure 5.1: Typical peptidoglycan structure of Gram-positive bacteria, showing lysin cleavage sites. The cleavage sites are indicated: (1) N-acetylmuramoyl-L-alanine amidase (2) L-alanoyl-D-glutamate endopeptidase (3) D-glutamyl-m-DAP endopeptidase (4) interpeptide bridge-specific endopeptidases (5) N-acetyl-b-D-glucosaminidase and (6) N-acetyl-b-D-muramidase.

The current thesis work provides insights into:

1. Structure-function analysis of calcium-bound and calcium-deficient PlyGRCS-*Ec*-CspC protein complex.
2. Biochemical studies to understand the interaction between *E. coli*-CspC, *S. aureus*-CspC, ssDNA, and PlyGRCS.
3. Microbial assays to check the role of Ca2+ cations and the active site residues of PlyGRCS endolysin in the lysis of MRSA.

This study throws light on the mechanism involved between PlyGRCS and CspC and also provides a molecular basis for the bacteriolytic activity of PlyGRCS against MRSA.

OBJECTIVE OF THE STUDY:

1. Structure, function, and microbial analysis of the Staphylococcus PhageGRCS Endolysin containing CHAP and SH3b domain,

a) Cloning in different vectors, expression, and purification of PlyGRCS endolysin protein from *E. coli* system.
b) Crystallization, X-ray diffraction, data collection, 3D structure determination, and analysis of calcium-bound and calcium-deficient PlyGRCS-*Ec*-CspC protein complex.
c) Site-directed mutagenesis studies for the identification of critical active site residues in the PlyGRCS.
d) Binding studies of *E. coli*-CspC, *S. aureus*-CspC, ssDNA, and PhageGRCS by using Micro-scale Thermophoresis.
e) Microbial assays of active site residues of PlyGRCS lytic activity against MRSA using Turbidity reduction assay & Disc diffusion assay.

CHAPTER – 6: MATERIAL AND METHODS

E. coli DH5α cells were grown in LB media with respective antibiotics for cloning and site-directed mutagenesis of recombinant genes (PlyGRCS, *E. coli* & *S. aureus* CspC). Clone confirmation was done by sequencing. Expression hosts, BL21 codon plus, and Rosetta *E. coli* cells were used for protein expression, followed by the production of PlyGRCS (wild type & mutants), *E. coli* & *S. aureus* CspC proteins were performed by a series of chromatographic techniques to get pure proteins. Protein homogeneity and stability were checked by Dynamic light scattering and Tycho. *S. aureus* (ATCC 29213), *S. saprophyticus* (ATCC 19701), *E. coli* (ATCC 25922), and methicillin-resistant *S. aureus* (MRSA) were used for microbial assays.

The purified PlyGRCS (wild type & mutants), *E. coli* & *S. aureus* CspC proteins were used for the binding studies by Microscale thermophoresis (MST) and microbial assays. The *E. coli* CspC form the protein complex was confirmed by Mass spectrometry.

PlyGRCS-*Ec*-CspC with or without calcium were crystallized by using hanging drop crystallization. X-ray diffraction data were collected on the beamline ID23 at ESRF, Grenoble, France. The X-ray data diffracted were merged, indexed, and integrated using iMosflm. (Powell et al., 2013) and scaled with *Aimless* from the CCP4 program package. The crystal structure was refined by using module *phenix. refine* of the *PHENIX* package (Adams et al., 2010). The Coot program (Emsley and Cowtan, 2004) Was used for tracing the protein chains on the electron density maps. The final structures and refined maps were visualized and illustrated using PyMOL v.1.3r. The MOLPROBITY program (Chen et al., 2010) was used to assess the stereochemistry of these crystal structures.

Binding studies were performed for the PlyGRCS (wild type & mutants), *E. coli* & *S. aureus* CspC by MST. Competitive binding studies were carried out for PlyGRCS, *E. coli* & *S. aureus* CspC, and ssDNA by MST.

Calcium interacting residues and catalytic active site residue mutants of PlyGRCS were taken for the microbial assays. To check the lytic activity of the wild-type and mutant PlyGRCS; microbial assays namely, turbidity reduction and disc diffusion assays were performed. Turbidity reduction assay where reduction in the turbidity of the *S. aureus* cells by different concentrations of PlyGRCS were recorded by absorbance at OD 600nm. Further, disc diffusion assay where the zone of inhibition were observed upon treatment with different amount of PlyGRCS on *S. aureus* grown plates.

CHAPTER -7: RESULTS AND DISCUSSION

OBJECTIVE 1:

- **Protein expression and production of PlyGRCS (wild type & mutants), *E. coli* and *S. aureus* CspC**

All the proteins were expressed on a large scale for protein purification. During Ni-NTA affinity purification, the full-length PlyGRCS protein was eluted in two peaks **(Figure 7.1).** In peak 1, PlyGRCS is co-eluted with an unknown small-size protein of ~7.5 kDa, and peak 2 has only one band corresponding to the PlyGRCS protein. We have attempted to crystallize both peak 1 and peak 2 independently and got crystals for peak 1 only.

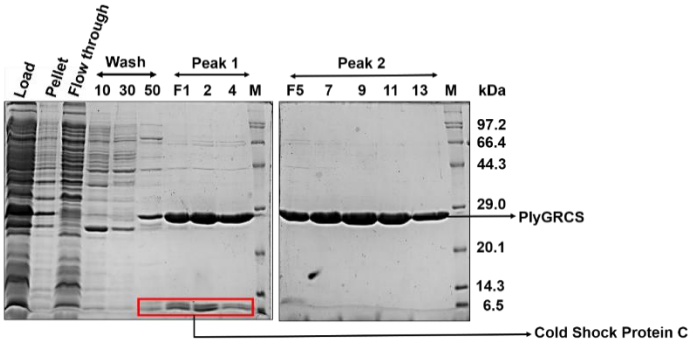

Figure 7.1: SDS-PAGE analysis of Ni-NTA purified PlyGRCS protein. The 'peak 1' fraction contains both PlyGRCS and *Ec*-CspC, while the 'peak 2' fraction contains PlyGRCS only.

- **Structure determination of PlyGRCS-*Ec*-CspC protein complex**

The X-ray data diffracted for calcium and without calcium PlyGRCS-*Ec*-CspC to 2.1 Å and 1.67 Å resolution. The calcium **(Figure 7.2A)** and without calcium **(Figure 7.2B)** PlyGRCS-*Ec*-CspC crystal was found to belong to the $P2_12_12_1$ space group (PDB ID: 8H1I) and C2 space group (PDB ID: 8XYF) respectively. The crystal structure of PlyGRCS contains the $CHAP_{GRCS}$ and $SH3_5_{GRCS}$ domains connected by a linker, 142-155aa. The $CHAP_{GRCS}$ domain (aa: 1-141) comprises a central six-stranded antiparallel β–sheet arranged in the topology of the β1β6β2β3β4β5 (Figure 1d). A Ca^{2+} ion is found in the L1 loop, which connects α1 and α2. The $SH3_5_{GRCS}$ domain of PlyGRCS comprises eight β-strands (β1-β8). During tracing the full-length of PlyGRCS on the 2m|Fo| - D|Fc| and the difference Fourier m|Fo| - D|Fc| maps, surprisingly, an additional electron density consistently appeared corresponding to a polypeptide fragment near the interface between the $CHAP_{GRCS}$ and $SH3_5_{GRCS}$ domains. Superposition of Calcium and calcium-deficient PlyGRCS-*Ec*-CspC complex revealed a major difference in the calcium-binding region in the CHAP domain of PlyGRCS **(Figure 7.2C).**

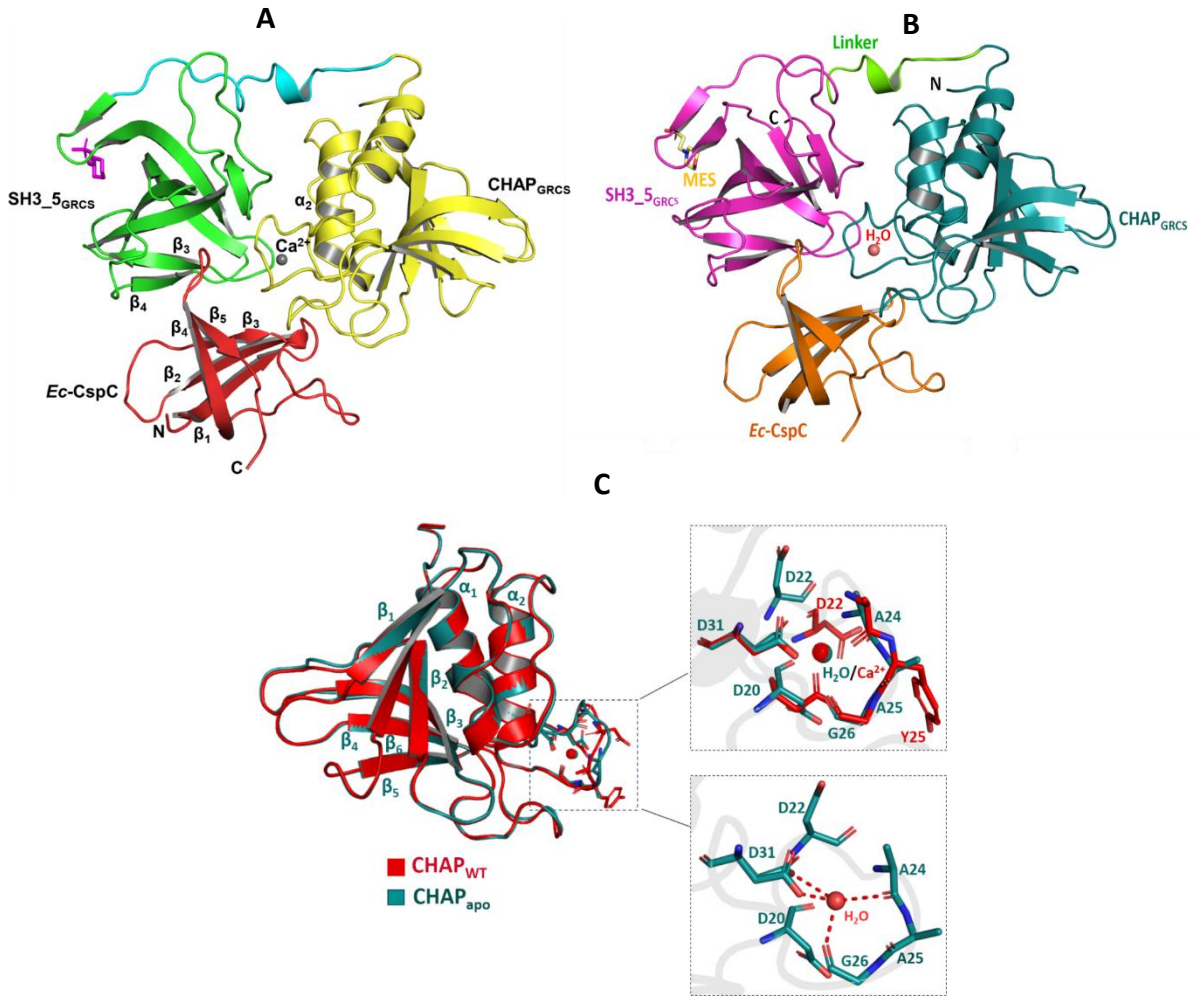

Figure 7.2: The crystal structure of the **A.** PlyGRCS – *Ec*-CspC complex. **B.** calcium deficient PlyGRCS – *Ec*-CspC complex. **C.** Superposition of the respective CHAP-domain of wild-type and Ca^{2+}-depleted $CHAP_{apo}$ domain of PlyGRCS. The interacting residues are shown by sticks.

- **Microscale thermophoresis (MST) of PlyGRCS (wild type & mutants), *E. coli* and *S. aureus* CspC**

Based on the PlyGRCS-*Ec*-CspC complex structure, a quantitative binding assay was performed between *Ec*-CspC and PlyGRCS (wild-type and mutants) to evaluate their binding efficiency. The specific residues mutated in the PlyGRCS are D22A, Q231A, and D22A+Q231A. The binding affinity of PlyGRCS with *Ec*-CspC showed a K_D value of 145 nM, while that for the mutants D22A, Q231A, and double mutant D22A+Q231A yielded K_D values of 167 nM, 1.89 µM, and 887 nM, respectively **(**The binding affinity of *Sa*-CspC with the PlyGRCS was determined to be 152 nM **(Figure 7.3 a-f).** To validate whether PlyGRCS inhibits the nucleic acid binding to CspC, a quantitative binding assay was again carried out for *Sa*-CspC and *Ec*-CspC with ssDNA. The binding affinity of *Sa*-CspC and *Ec*-CspC with the ssDNA was 714 nM and 677 nM, respectively **(Figure 7.4 A & B).**

Next, to understand whether PlyGRCS-CspC interaction blocks the nucleic-acid binding of CspC, the author carried out a quantitative binding assay of the above complex with ssDNA. For this study, *Sa*-CspC was mixed with an increasing concentration of PlyGRCS (1:1 and 1:2 ratio), then the complex was studied for its interaction with ssDNA **(Figure 7.4 C & D).**

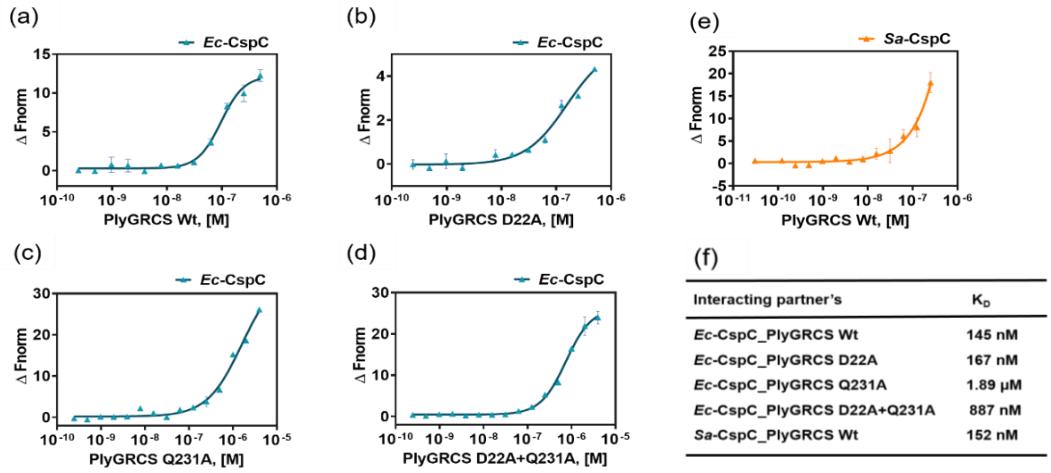

(f)

Interacting partner's	K_D
Ec-CspC_PlyGRCS Wt	145 nM
Ec-CspC_PlyGRCS D22A	167 nM
Ec-CspC_PlyGRCS Q231A	1.89 µM
Ec-CspC_PlyGRCS D22A+Q231A	887 nM
Sa-CspC_PlyGRCS Wt	152 nM

Figure 7.3: MST analysis of *Ec*-CspC interactions with PlyGRCS (wild-type (Wt) and mutants) proteins. Binding curves for the interactions of fluorescently labeled *Ec*-CspC with (a) Wt-PlyGRCS, (b) D22A PlyGRCS. (c) Q231A PlyGRCS. (d) D22A+Q231A PlyGRCS, and the interaction of fluorescently labeled *Sa*-CspC with (e) Wt PlyGRCS were shown as the change in normalized fluorescence (ΔFnorm). The K_D values are summarized in the Table. The K_D values were obtained after fitting the binding curves between ΔF_{norm} plotted as a function of the ligand concentration. The values are plotted on normalized fluorescence (y-axis) against increasing concentrations (x-axis). Error bars represent SEM (n = 3)

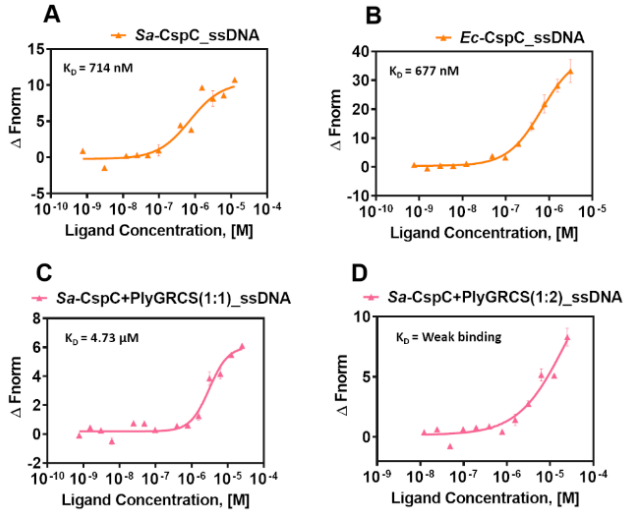

Figure 7.4: MST analysis of *Sa*-CspC, *Ec*-CspC, and PlyGRCS interactions with ssDNA. Binding curves for the interactions of fluorescently labeled (a) *Sa*-CspC and (b) *Ec*-CspC, respectively, with ssDNA were shown as the change in normalized fluorescence (ΔFnorm). Binding curves for the interactions of fluorescently labeled (c) *Sa*-CspC+PlyGRCS complex (1:1 ratio) and (d) *Sa*-CspC+PlyGRCS complex (1:2 ratio), respectively, with ssDNA were shown as the change in normalized fluorescence (ΔFnorm). The K_D values were obtained after fitting the binding curves

between ΔF_{norm} plotted as a function of the ligand concentration. The values are plotted on normalized fluorescence (y-axis) against increasing concentrations (x-axis). Error bars represent SEM (n = 3)

- **Turbidity reduction assay (Lytic Activity) for PlyGRCS**

Turbidity reduction assays were performed to evaluate the lytic activity of PlyGRCS against ATCC 29213 *S. aureus*, MRSA, and the non-specific Gram-positive *S. saprophyticus* and Gram-negative *E. coli* bacterial strains as controls **(Figure 7.5).** The lytic activity was measured based on turbidity reduction by using a spectrophotometer. The PlyGRCS showed significant lytic activity against ATCC 29213 *S. aureus* at varying concentrations from 1.25 – 80 µg/ml **(Figure 7.5A).** Significant lytic activity was also observed for MRSA at the standardized minimal and maximal concentrations (10 µg/ml and 80 µg/ml) of PlyGRCS **(Figure 7.5B).** The lytic activity in the controls was nearly absent **(Figure 7.5C)**, suggesting that PlyGRCS is specific to *S. aureus* isolates. Turbidity reduction assay was also carried out for active site residue mutants PlyGRCS.

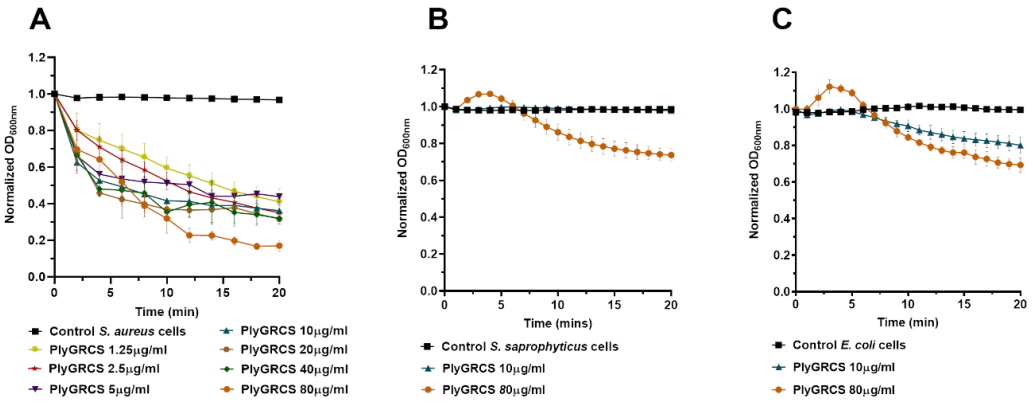

Figure 7.5: Lytic activity of PlyGRCS against *S. aureus* and controls by turbidity reduction assay. PlyGRCS was treated in a concentration-dependent manner from 1.25 µg/ml to 80 µg/ml against (A) *S. aureus* and with 10 µg/ml and 80 µg/ml concentrations against (B) *S. saprophyticus*, and (C) *E. coli.*

- **Disc diffusion assay or spot test assay**

To further evaluate the antibacterial activity of the purified proteins, we carried out a Disc-diffusion assay on *S. aureus* and MRSA **(Figure 7.6a,b)** and also PlyGRCS-*Ec*-CspC complex (peak 1) against *S. aureus* **(Figure 7.6c).** Protein spots (80, 40, 20, and 10 µg) were applied, and the strength of lytic zones was evaluated qualitatively. In contrast, PlyGRCS is host-specific as evidenced by the lack of lytic activity in non-specific hosts *S. saprophyticus* and *E. coli* **(Figure 7.6d,e).** Disc diffusion assay was also carried out for active site residue mutants PlyGRCS.

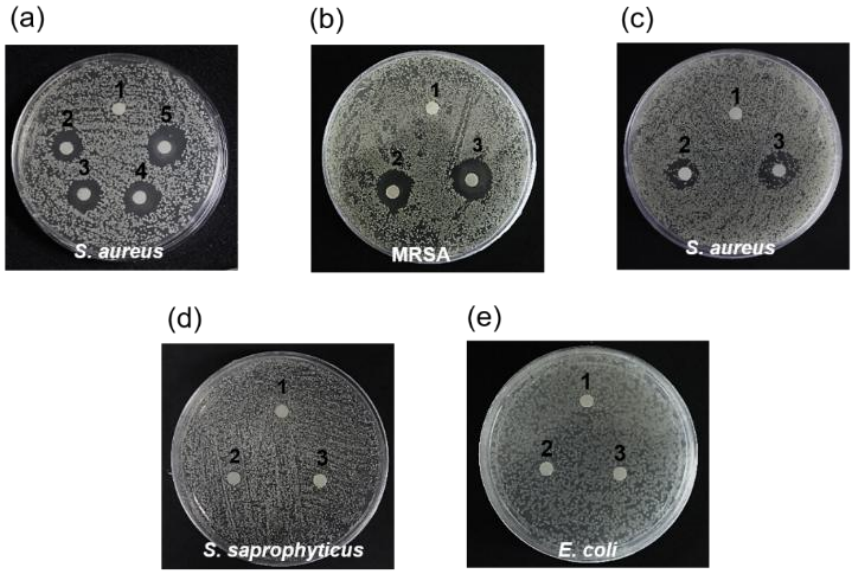

Figure 7.6: Disc diffusion assay of PlyGRCS against *S. aureus* isolates. PlyGRCS was treated against (a) *S. aureus* with amounts of (2) 10 µg, (3) 20 µg, (4) 40 µg, and (5) 80 µg. (b) MRSA with amounts of (2) 10 µg, and (3) 80 µg. (c) PlyGRCS-*Ec*-CspC (peak1) was treated against *S. aureus* with an amount of (2) 10 and (3) 80 µg. PlyGRCS was treated against (d) *S. saprophyticus* with amounts of (2) 10 µg and (3) 80 µg, and (e) *E. coli* with amounts of (2) 10 µg and (3) 80 µg. In all panels (a)-(e), #1 represents the control (protein buffer only).

CHAPTER – 8: CONCLUSION

Affinity purification of PlyGRCS yielded two peaks, peak 1 with PlyGRCS-Ec-CspC and peak 2 with PlyGRCS only. Peak 1 was taken for crystallization and peak 2 for microbial assays to check the lytic activity against MRSA strains.

Crystals were grown for Peak1, X-ray diffraction data was collected and the structure was analyzed. Along with the full-length PlyGRCS structure, an additional electron density consistently appeared corresponding to a polypeptide fragment near the interface between the $CHAP_{GRCS}$ and $SH3_5_{GRCS}$ domains. The final tracing of the polypeptide chain revealed that it is a cold shock protein CspC from the host bacteria, *E. coli*. To further confirm whether the bound protein with PlyGRCS is indeed *Ec*-CspC, we performed in-gel digestion for mass spectrometry analysis. The results obtained from this study further reiterated that the peptide sequence (Figure S1) was specific to that of *Ec*-CspC. Therefore, while expressing the PlyGRCS in the expression host, *E. coli* CspC is bound with the PlyGRCS.

To evaluate their binding efficiency, a quantitative binding assay was performed between Ec-CspC and PlyGRCS (wild-type and mutants). The binding affinity of PlyGRCS with *Ec*-CspC showed a K_D value of 145 nM, while that for the mutants D22A, Q231A, and double mutant D22A+Q231A yielded K_D values of 167 nM, 1.89 µM, and 887 nM,

respectively. Also, *S. aureus* CspC binding with PlyGRCS showed a K_D value of 152 nM. The K_D value of *E. coli* and *S. aureus* CspC are the same which implies that both CspC might similarly interact with PlyGRCS.

A quantitative binding assay was carried out for *Sa*-CspC and *Ec*-CspC with ssDNA. The binding affinity of *Sa*-CspC and *Ec*-CspC with the ssDNA was 714 nM and 677 nM, respectively. Both *Sa*-CspC and *Ec*-CspC showed a similar binding affinity for ssDNA. The binding affinity of ssDNA with *Sa*-CspC in the presence of PlyGRCS (1:1 and 1:2 ratio) yielded a K_D value of 4.73 μM and weak/no binding, respectively. This study revealed that PlyGRCS significantly blocks the binding of CspC with ssDNA.

Microbial assays were performed for the wild-type and active site mutants of PlyGRCS. Turbidity reduction and disc diffusion assay revealed that wild-type PlyGRCS showed good lytic activity against MRSA strains. The active site mutants of PlyGRCS showed no lytic activity or weak lytic activity against MRSA strains, which confers that the specific residues are important for the lytic activity of PlyGRCS.

REFERENCES:

1. Daniel C. Osipovitch, Sophie Therrien & Karl E. Griswold (2015) Discovery of novel S. aureus autolysins and molecular engineering to enhance bacteriolytic activity. Appl Microbiol Biotechnol. 99(15): 6315–6326.
2. Parisien A, Allain B, Zhang J, Mandeville R & Lan, C.Q (2008) Novel alternatives to antibiotics: bacteriophages, bacterial cell wall hydrolases, and antimicrobial peptides. J. Appl. Microbiol. 104, 1–13.
3. S.B. Linden, H. Zhang, R.D. Heselpoth, Y. Shen, M. Schmelcher, F. Eichenseher & D.C. Nelson (2015) Biochemical and biophysical characterization of PlyGRCS, a bacteriophage endolysin active against methicillin-resistant *Staphylococcus aureus*, Appl. Microbiol. Biotechnol. 99, 741–752.
4. Lood, R., Raz, A., Molina, H., Euler, C.W., and Fischetti, V.A (2014) A highly active and negatively charged *Streptococcus pyogenes* lysin with a rare D-alanyl-L-alanine endopeptidase activity protects mice against *streptococcal* bacteremia. *Antimicrob. Agents Chemother.*, 58 (6), 3073–3084.
5. Gu, J., Feng, Y., Feng, X., Sun, C., Lei, L., Ding, W., Niu, F., Jiao, L., Yang, M., Li, Y., Liu, X., Song, J., Cui, Z., Han, D., Du, C., Yang, Y., Ouyang, S., Liu, Z.-J., and Han, (2014) W. Structural and biochemical characterization reveals LysGH15 as an unprecedented "EF-hand-like" calcium-binding phage lysin. *PLoS Pathog.*, 10 (5): e1004109.
6. Powell HR, Johnson O, Leslie AGW. Autoindexing diffraction images with iMosflm. Acta Crystallogr. D Biol. Crystallogr. 2013;69:1195–1203.

7. Adams PD, Afonine PV, Bunkóczi G, Chen VB, Davis IW, Echols N, et al. PHENIX: a comprehensive Python-based system for macromolecular structure solution. Acta Crystallogr. D Biol. Crystallogr. 2010; 66:213–221.
8. Chen VB, Arendall WB, Headd JJ, Keedy DA, Immormino RM, Kapral GJ, et al. MolProbity: all-atom structure validation for macromolecular crystallography. Acta Crystallogr. D Biol. Crystallogr. 2010.;66:12–21.

PAPERS PUBLISHED:

- **Krishnappa G,** Nagaraj H, SureshKumar HB, Mandal M, Padavattan S, Bahubali VH, **Thiyagarajan S,** Padmanabhan B. Structural Basis for the Essential Role of Ca^{2+} in the Lytic Activity of *Staphylococcus aureus* PlyGRCS Endolysin Targeting Methicillin-Resistant *Staphylococcus aureus.* **Proteins. 2024** Dec 11. doi: 10.1002/prot.26777
- **Krishnappa G**, Mitali Mandal, Saranya Ganesan, Sudhagar Babu, Padavatan Sivaraman, Veena kumari HB & Balasundaram Padmanabhan, **(2023).** Structural and biochemical insights into the bacteriophage PlyGRCS endolysin targeting methicillin-resistant *Staphylococcus aureus* (MRSA) and serendipitous discovery of its interaction with a cold shock protein C (CspC) from *E. coli.* **Protein Science, 2023**.Sep;32(9):e4737, doi: 10.1002/pro.4737
- Unni S, Deshmukh P, **Krishnappa G**, Bharath MMS, Padmanabhan B. Chlorhexidine as a Keap1-Nrf2 inhibitor: a new target for an old drug for Parkinson's disease therapy. J Biomol Struct Dyn. **2023** Jul-Aug;41(12):5367-5381. doi: 10.1080/07391102.2022.2086175.
- Unni S, Deshmukh P, **Krishnappa G**, Kommu P, Padmanabhan B. Structural insights into the multiple binding modes of Dimethyl Fumarate (DMF) and its analogs to the Kelch domain of Keap1. FEBS J. **2021** Mar;288(5):1599-1613. doi: 10.1111/febs.15485.
- Deshmukh P, Mathur S, Gangadharan G, **Krishnappa G**, Dalavaikodihalli Nanjaiah N, Padmanabhan B. Novel pyrano 1,3 oxazine-based ligand inhibits the epigenetic reader hBRD2 in glioblastoma. Biochem J. **2020** Jun 26;477(12):2263-2279. doi: 10.1042/BCJ20200339
- **Gopinatha et al,** Phenanthradine derived inhibitors against BTB domain of Keap1: novel drug therapeutics implication in neurodegenerative diseases (**Manuscript under preparation**)
- **Gopinatha et al,** Investigation of therapeutic potential of phytochemicals from Nardostachys jatamansi against neurodegenerative diseases (**Manuscript under preparation**)
- **Gopinatha et al,** Understanding the molecular mechanism involved in the interaction of BTBIVR domain of Keap1 with Cullin3 protein (**Manuscript under preparation**)